Thorium aspartate tetrahydrate precursor to ThO 2 : Comparison of hydrothermal and thermal conversions

Nicolas Clavier, Jérôme Maynadie, Adel Mesbah, J. Hidalgo, R. Lauwerier, G.I. Nkou Bouala, Sandra Parrès-Maynadié, D. Meyer, N. Dacheux, Renaud Podor

Thorium Aspartate Tetrahydrate Precursor to ThO_2 : Comparison of Hydrothermal and Thermal Conversions

N. Clavier [1,], J. Maynadié [1], A. Mesbah [1], J. Hidalgo [1], R. Lauwerier [1], G.I. Nkou Bouala [1], S. Parrès-Maynadié [1], D. Meyer [1], N. Dacheux [1], R. Podor [1]*

[1] ICSM, Institut de Chimie Séparative de Marcoule, UMR 5257 CEA/CNRS/UM/ENSCM, Site de Marcoule – Bât. 426, BP 17171, 30207 Bagnols/Cèze cedex, France

*** Corresponding author :**

Dr. Nicolas CLAVIER
ICSM – UMR 5257 CEA/CNRS/UM/ENSCM
Site de Marcoule – Bât 426
BP 17171
30207 Bagnols sur Cèze
France

Phone : + 33 4 66 33 92 08
Fax : + 33 4 66 79 76 11

nicolas.clavier@icsm.fr

Abstract :

The synthesis of original crystalline thorium aspartate tetrahydrate, $Th(C_4NO_4H_6)_4.4H_2O$, was performed using two different wet-chemistry routes, involving either L-asparagine or L-aspartic acid as complexing agent. Characterization of this compound through ^{13}C NMR and PXRD led to confirm the terminal coordination mode of the aspartate group and to suggest a potential cubic lattice (Pn-3 space group). Vibrational spectroscopy data were also collected. The conversion of thorium aspartate tetrahydrate into thorium dioxide was further performed through classical high temperature heat treatment or under hydrothermal conditions. On the one hand, thermal treatment provided a pseudomorphic conversion which retained the starting morphology, and favored the increase of the average crystallite size, as well as the complete elimination of the residual carbon content. On the other, hydrothermal conversion could be used to tune the morphology of the final oxide, $ThO_2.nH_2O$ microspheres being prepared when starting from L-asparagine.

Keywords :

Thorium – molecular complex – conversion – thorium oxide – hydrothermal

1. Introduction

Actinide carboxylates have been studied for long as precursors for high-temperature phases such as $An^{III}_2O_3$ and $An^{IV}O_2$ [1], or AnC carbides through direct carbothermic reduction [2]. In the case of oxides, they are easily converted by heating that allows both dehydration and decomposition of the low-temperature phases. Moreover, such a transition was frequently reported to preserve the original morphology of the low-temperature phase used, leading to so-called pseudomorphic transformations. Among the wide bunch of precursors explored in the literature, oxalate compounds were probably the most investigated [3-6]. Indeed, oxalic precipitation of tri- and/or tetravalent actinides generally provides high recovery yields associated with rapid kinetics, and produces powders with a good sintering capability [7-9]. More recently, more sophisticated ligands were used to form original solid phases [10-12]. Also, the choice of the ligand can be optimized to orientate the morphology of the precipitated powder [13].

Indeed, shape-controlled oxides constitute a great challenge for actinide-based materials [14] regarding to their interesting properties. As instance, uranium oxide nanospheres have already attracted some attention in view of their catalytic properties, particularly in the framework of the destruction of volatile organic compounds [15]. More importantly, as actinide oxides constitute one of the reference fuel for the current nuclear reactors, several future Gen IV concepts [16], and alternate reactors based on the thorium fuel-cycle [17, 18], the design of spherical actinide dioxides could allow the preparation of powders with interesting properties, such as improved flowability. Hence, while lanthanide oxides were already prepared under very various shapes such as nanotubes, nano- or micro-rods, thin films … actinides compounds were frequently limited to spheres [19-21]. Also, literature mainly addressed uranium-based samples, with very few synthesis routes toward other actinide oxides with controlled morphology, including ThO_2 [22, 23].

This paper then reports the first study concerning the use of a simple amino acid (asparagine) and its derivative (aspartic acid) to prepare crystallized precursor of thorium dioxide. The main objective is to control the final ThO_2 morphology both through synthesis conditions and conversion processes. Amino acids were selected as precipitating agents, owing to their good complexation properties regarding actinides, as attested by their role in the bioaccumulation of thorium and uranium in several micro-organisms such as yeasts or mycobacteria [24, 25]. Also, asparagine was recently used during the synthesis of lanthanide

coordination polymers that can adopt various morphologies depending on the polarity of the solvent used [26, 27]. The thorium-based compounds obtained using either asparagine or aspartic acid were first characterized, both from morphological and physico-chemical point of views (including structural and spectroscopic aspects), while their decomposition into dioxide was further studied. On the one hand, a classical thermal decomposition was performed. Nevertheless, if such a heat treatment generally keeps the starting morphology of the samples unchanged, it can lead to important modifications in their microstructural properties. As a matter of example, the surface reactivity of the powders is frequently modified, either through the formation of mesoporosity during the decomposition of the organic part of the initial precursor, or during its progressive elimination subsequently to grain growth [28]. The crystallinity of the oxide produced was also reported to be drastically impacted by the thermal heat treatment, which can further modify the ability of the powders towards sintering. Finally, depending on the atmosphere used during the conversion, the elimination of residual carbon coming from the decomposition of organics might be incomplete [29]. In order to overcome such potential issues, hydrothermal decomposition of the precursor was then undertaken, with the aim to simultaneously tune the morphology of the powders and to achieve their transformation towards the oxide form with original microstructures. Such features can finally be used to optimize some of the properties of interest of ThO_2-based materials, such as sintering capability [8], homogeneity or chemical durability [30, 31].

2. Experimental section

2.1. Preparation of the samples

All the reagents used were of analytical-grade and supplied by Sigma-Aldrich, including thorium nitrate pentahydrate. The synthesis of thorium-based compounds was adapted from the protocol previously reported by Shen *et al.* [26] for the preparation of CeO_2 powders with controlled morphology. A mixture of thorium nitrate pentahydrate (typically 1.4×10^{-3} mole) and L-asparagine ($C_4H_8N_2O_3$, 6×10^{-4} mole) with molar ratio A/Th ~ 0.4 was dissolved in 10 mL of deionized water then poured in a PTFE-lined autoclave supplied by Parr company. The resulting pH was measured around 2. A heat treatment at 160°C was further performed for 24 hours and yielded to a white precipitate. A second protocol was developed by replacing L-asparagine by aspartic acid ($C_4H_7NO_4$) (**Figure 1**), still considering the same molar ratio. The pH of the starting mixture was not significantly modified compared to the previous case and remained close to 2. In these conditions, and owing to the pKa values of aspartic acid [32], the main species in solution should be $(C_4H_6NO_4)^-$. For all the samples prepared, the solid phase was finally separated from the supernatant by centrifugation, washed several times with deionized water then ethanol, and finally dried overnight at room temperature under a fume hood.

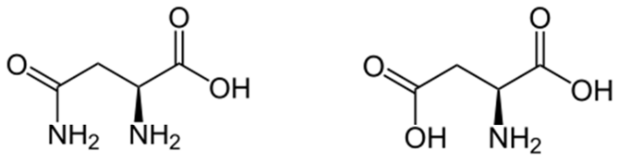

L-asparagine **L-aspartic acid**

Figure 1. Chemical structure of L-asparagine and L-aspartic acid ligands.

2.2. Characterization

Chemical analyses. Nitrogen and oxygen contents in the starting aspartate precursors were evaluated using a LECO TCH600 apparatus. In order to get quantitative values, a blank then a series of standards (including steels with controlled amount of O and N, as well as HfO_2) were analysed prior to our samples. Similarly, the amount of carbon in the oxide powders was

evaluated by the means of a LECO CS230 analyser, using the complete combustion of the samples in a large excess of O_2 followed by a mass spectrometer measurement of CO_2. Unfortunately, under these conditions, the combustion of the aspartate precursors was found to be incomplete and precluded a reliable determination of the carbon content.

ESEM observations. Prior to their observation, the samples were dispersed in acetone and deposited on a carbon sample holder. Environmental scanning Electron Microscope (ESEM) micrographs were directly recorded from the as-deposited powders without additional preparation such as metallization. A FEI Quanta 200 environmental scanning electron microscope, equipped with a Large Field Detector (LFD) and a Back-Scattered Electron Detector (BSED), was used to record the images. A low acceleration voltage of 5-10 kV coupled with low vacuum conditions (80 Pa water vapor) was chosen to observe the samples in order to prevent their degradation under the electron beam.

High Temperature ESEM observations. Direct ESEM observations of the samples were performed at high temperature using a specific high temperature stage that can be attached to the ESEM. The samples were dispersed in acetone. One drop of the mixture was deposited on a 2 $mm^2 \times 0.2$ mm height platinum sample holder and transferred in the high temperature stage. Then, it was heated from RT to 800°C with a 10°C heating rate, while continuously recording high magnification images on selected crystals. The air pressure in the ESEM chamber was kept to 300 Pa during the experiment. Image processing was performed using the Fiji software [33].

NMR. MAS NMR measurements were performed on a Bruker Avance III 400 spectrometer, equipped with a 4 mm MAS probe 1H/X. Samples were packed into zirconia rotors and spun at 12 kHz at room temperature. ^{13}C and ^{15}N NMR spectra were recorded using TMS and CH_3NO_2 (liq.) as references, respectively. ^{13}C and ^{15}N CP-MAS (Cross Polarization) experiments were performed with a contact time of 2 ms and recycle delays of 5 s and 2 s, respectively.

Vibrational spectroscopy. Raman spectra were recorded by the means of a Horiba - Jobin Yvon Aramis apparatus equipped with an edge filter and using a Nd:YAG laser (532 nm) delivering 60 mW on the sample surface. The laser beam was focused on a small fraction of powdered sample simply deposited on a glass lamella using an Olympus BX 41 microscope.

A ×100 objective with a numerical aperture of 0.9 was used, resulting in a spot size of about 1 μm^2. The scattered Raman light was collected in a 180° backscattering geometry and dispersed by a grating of 1800 grooves/mm after having passed a 150 µm entrance slit, resulting in a spectral resolution lower than 1 cm^{-1}. For each spectrum, a dwell time of 2 to 5 seconds was considered with an average of 3 scans. Before analysis, the apparatus was calibrated with a silicon wafer, using the first-order Si line at 520.7 cm^{-1}.

Attenuated Total Reflectance Fourier Transform InfraRed (ATR-FTIR) spectra were recorded in the 380-4000 cm^{-1} range thanks to a Perkin-Elmer FTIR Spectrum 100 device. Powdered samples were deposited at the surface of the single bounce diamond crystal ATR accessory without any prior preparation. The spectra collected in such operating conditions exhibited a resolution lower than 2 cm^{-1}.

PXRD. Powder X-Ray Diffraction (PXRD) diagrams were obtained by the means of a Bruker D8 diffractometer equipped with a Lynx-eye detector adopting the reflexion geometry and using Cu $K\alpha_{1,2}$ radiation (λ = 1.54184 Å). PXRD patterns were recorded at room temperature in the $5° \leq 2\theta \leq 120°$ range, with a step size of $\Delta(2\theta) = 0.03°$ and a total counting time of about 1.5 hours per sample. Powders were staggered on stainless steel sample holders ($C_{0.05}Fe_{0.95}$, space group Fm-3m, PDF file #00-023-0298) for analysis purposes.

On the one hand, thorium aspartate samples were refined by Le-Bail method. Only the unit cell parameters were refined after the indexation of the corresponding powder pattern. On the other hand, all the PXRD patterns corresponding to the oxides ThO_2 were refined by the Rietveld method using the Cox-Hastings pseudo-Voigt profile function [34] implemented in the Fullprof_suite program [35]. During all the refinements, the conventional profile/structure parameters were allowed to vary, i.e. zero shift, unit cell parameters, scale factors and a global thermal displacement. Moreover, the modelling of the intrinsic microstructure parameters was performed for each phase by applying an anisotropic size model.

TG-DT Analyses. Thermogravimetric analyses were undertaken thanks to a Setaram Setsys Evolution equipped with a type-S thermocouple (Pt / Pt-10%Rh). After recording the baseline using an empty crucible (100 µL), the weight loss was measured during a heat treatment up to 1000°C with a rate of 10°C.min^{-1}. Moreover, the gaseous species emitted during the heat treatment were analysed by the means of Hiden Analytical QGA analyser using mass spectrometry.

3. Results and discussion

3.1. Characterization of thorium aspartate samples

Electron microscopy. ESEM observations of the samples prepared revealed the systematic formation of well-defined objects with a bipyramidal shape, which can be considered as single-crystals. Their size typically varied from 2 to 10 µm and was not significantly affected by the nature of the complexing reagent used (*i.e.* L-aspartic acid or L-asparagine). Also, the crystals presented a strong tendency to aggregation, with the formation of agglomerates through face to face assemblies.

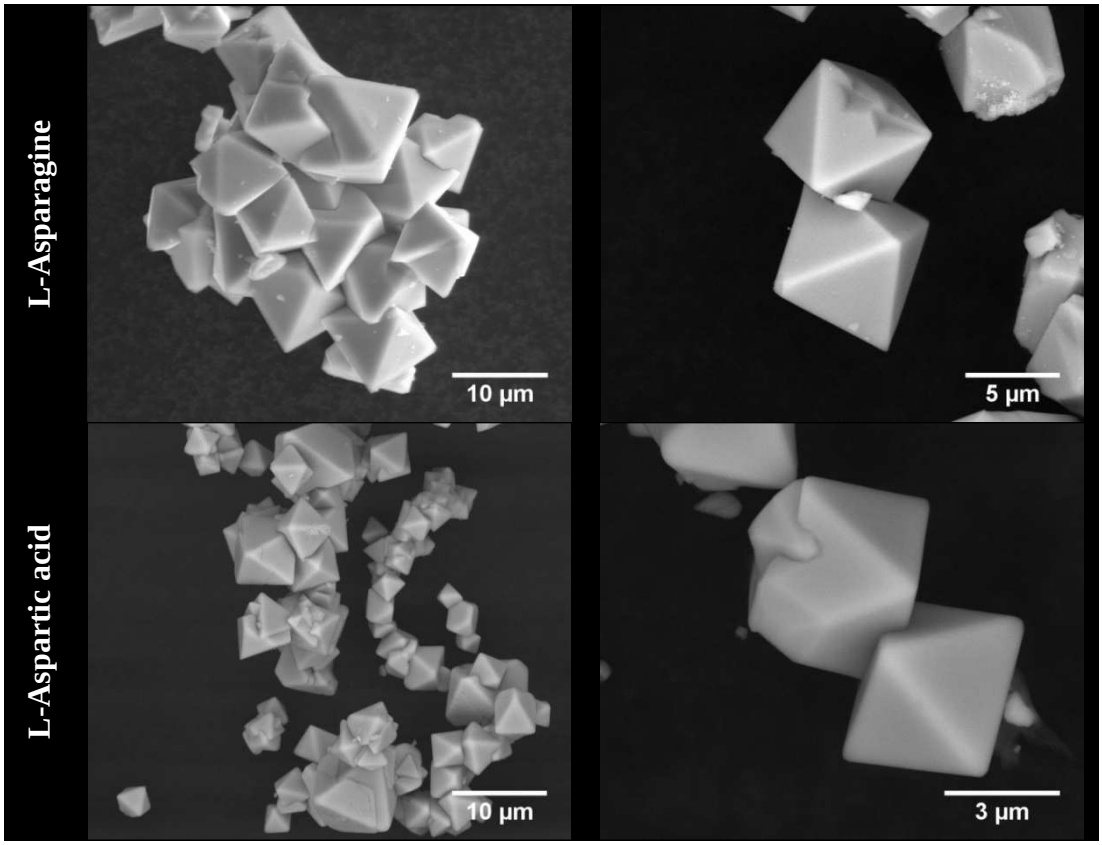

Figure 2. ESEM micrographs of the precipitates obtained after complexation of thorium with asparagine or aspartic acid.

Solid state NMR. The samples were analyzed by ^{13}C and ^{15}N solid state NMR along with pure L-asparagine or L-aspartic acid for comparison purposes. Two signals were observed at around 175 ppm on the ^{13}C NMR spectra of the two organic compounds considered and were attributed to the carbonyl fragments of amide or carboxylic moieties (**Figure 3**). For the

synthesized Th-based samples, two signals were observed at 171.72 ppm and 136.84 ppm. The chemical shift of the former one is characteristic of a non-coordinated carbonyl moiety in comparison with pure asparagine or aspartic acid spectra. The offset observed for the second one ($\Delta\delta \approx 40$ ppm) can be attributed to the complexation with thorium. These observations can then be related to the formation of thorium molecular species through interaction with only one carbonyl fragment.

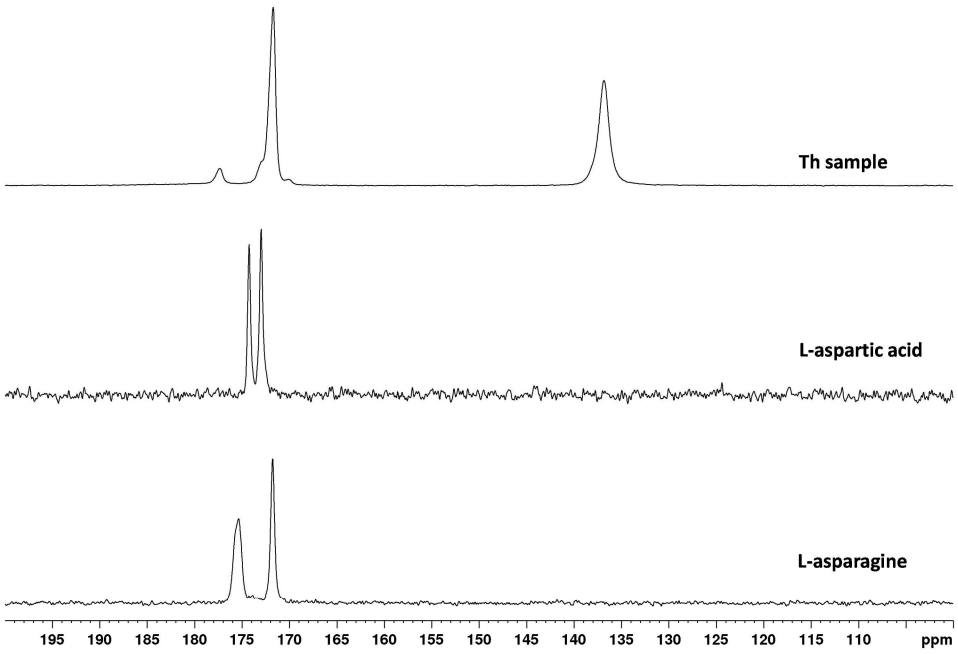

Figure 3. Solid state ^{13}C NMR CP-MAS spectra of L-asparagine, L-aspartic acid and Th sample in the 200-100 ppm range (full spectra are supplied as supplementary material).

Analysis of the ^{15}N NMR spectra of the pure organic compounds enabled the assignment of the different signals (**Figure 4**). On the one hand, the signal at -265.39 ppm, only observable on the L-asparagine spectrum, was assigned to the amide fragment. On the other hand, all the spectra exhibited a signal around -340 ppm, which was assigned to the amine moiety in α-position of the carbonyl group. This signal was also present at -347.54 ppm on the glycine spectrum which was used as a reference for ^{15}N NMR calibration experiments. Similarly to L-aspartic acid, all the spectra recorded for the Th-based samples only presented one signal around -340 ppm. The lack of signal around -265 ppm on thorium-based samples spectra synthesized with asparagine could be attributed to the *in situ* conversion of asparagine into aspartic acid before the complexation with the metal center.

Indeed, hydrolysis mechanism of asparagine under hydrothermal conditions was already reported by Chen *et al.* during the synthesis of nanostructured $In(OH)_3$ spheres [36]. Based on these results, the samples prepared under hydrothermal conditions are probably composed of thorium aspartate complexes, whatever the organic precursor initially used (asparagine or aspartic acid).

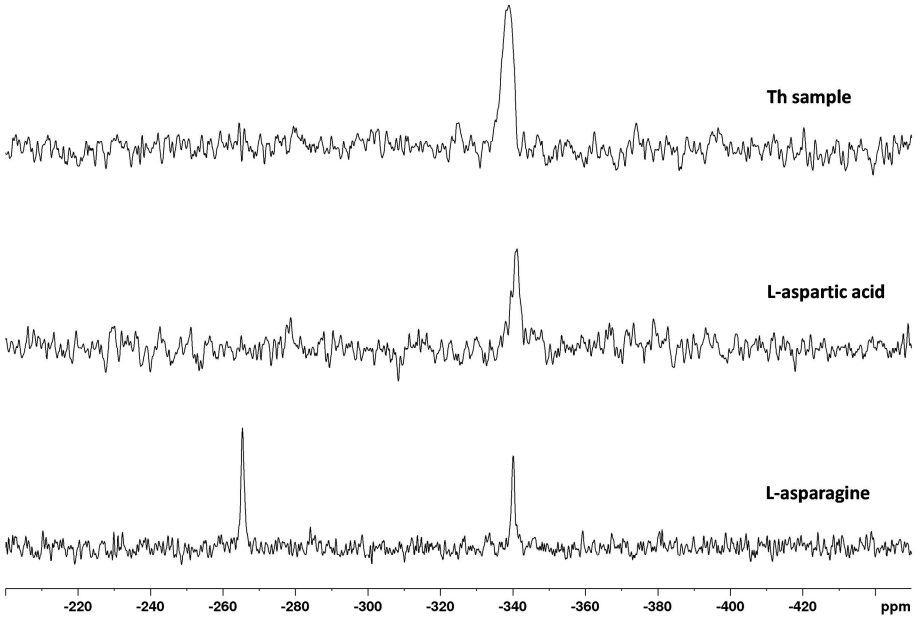

Figure 4. Solid state ^{15}N NMR CP-MAS spectra of L-asparagine, L-aspartic acid and Th sample in the -200 to -450 ppm range.

Vibrational spectroscopy. Samples were further characterized by ATR-FTIR and Raman spectroscopies (**Figure 5**). Pure L-asparagine and L-aspartic acid were also analysed for comparison purposes. For the two ligands, the characteristic features already reported in the literature were evidenced [37, 38]. Among the numerous vibration modes observed (see Tables S1 and S2 supplied as supplementary material for detailed assignment), both L-asparagine and L-aspartic acid exhibited intense bands corresponding to CO_2^- bending modes (typically in the 600-800 cm^{-1} range) as well as C-C (900-1000 cm^{-1}) and NH_2 (above 3000 cm^{-1}) stretching vibrations. Nevertheless, their spectra significantly differed when considering the bands assigned to the amide group. Indeed, the vibration modes assigned to C-N stretching (around 1400 cm^{-1}), NH_2 bending (1600-1630 cm^{-1}) and anti-symmetrical stretching (3350 cm^{-1}) were only pointed out in the spectra recorded for asparagine.

(a)

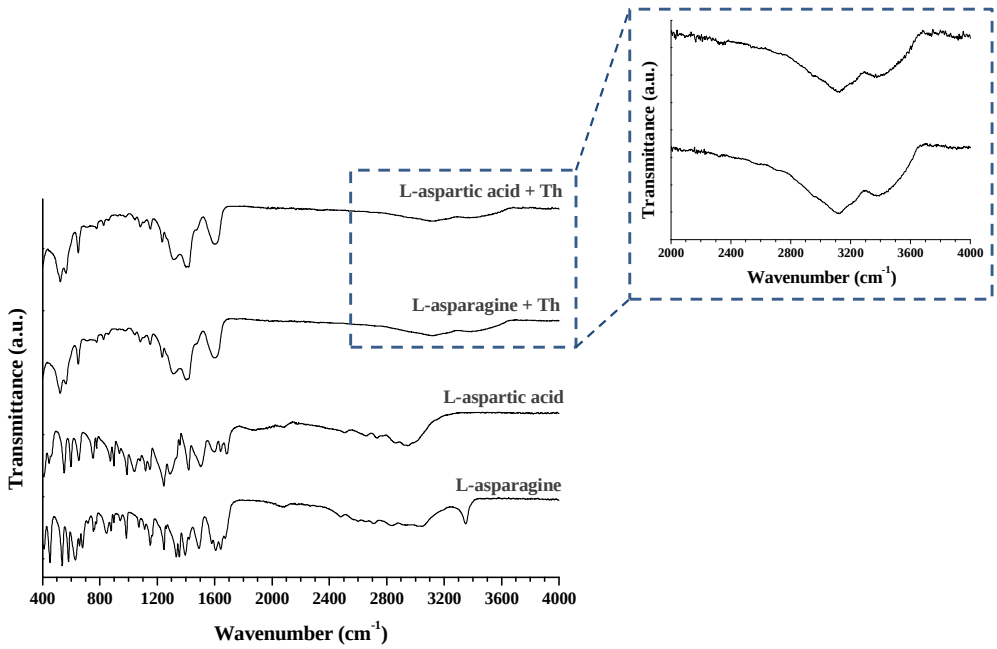

(b)

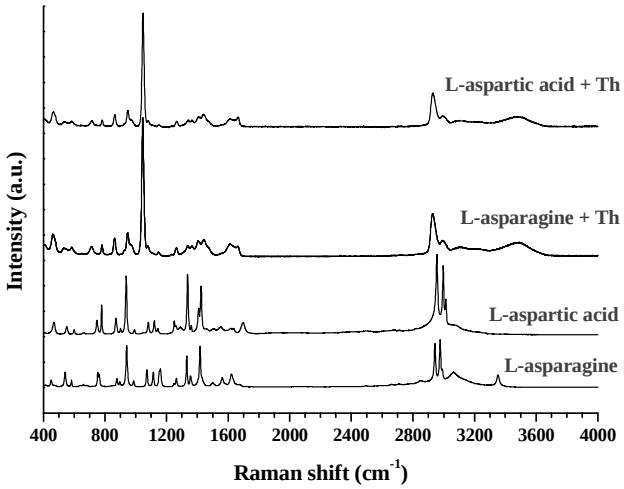

Figure 5. ATR-FTIR (a) and Raman (b) spectra recorded for precipitates prepared after complexation of thorium solution with L-asparagine and L-aspartic acid and comparison with pure ligands.

Conversely, ATR-FTIR and Raman spectra recorded for the thorium-based compounds were found to be entirely similar whatever the method of preparation employed. Moreover, similarly to L-aspartic acid, they did not present any vibration band characteristic of the amide group. This result is then in good agreement with that obtained from ^{15}N NMR and evidenced the deamidation of asparagine under the synthesis conditions [36]. On the basis of the data recorded for pure ligands, and by analogy with other metallic aspartates such as hydroxo-aqua nickel (II) [39], an attempted assignment of the vibration bands observed for

the complexes prepared is proposed in **Table 1**. Besides the characteristic modes already discussed for pure aspartic acid, the presence of water in the prepared compounds was also clearly evidenced, particularly from the large and intense band observed around 3500 cm^{-1} in both ATR-FTIR (see insert on **Figure 5a**) and Raman spectra. On this basis, one can definitely conclude that the samples prepared from the two synthesis routes investigated are thorium aspartate hydrate complexes, with the general formula $Th(C_4NO_4H_6)_4.nH_2O$.

Table 1. Assignment of the bands observed in the ATR-FTIR and Raman spectra recorded from thorium complexes with asparagine and aspartic acid.

ATR-FTIR (cm^{-1})	**Raman (cm^{-1})**	**Assignment**
	466	τ (NH_2)
523	537	δ_s (OCO)
562	585	
649	715	δ_{as} (OCO)
778	783	γ (OCO)
827		ω (H_2O)
861	863	γ (NH_2)
978	949	ν (CC)
	974	
1082	1047	ν (CN)
	1082	
1151	1150	r (NH_2)
1235	1266	t (CH_2)
1266		
1312		ν (CO)
	1341	δ (CH)
	1366	
1400	1407	ν_s (OCO)
1417	1443	
1476		δ_s (NH_2)
1600	1612	ν_{as} (OCO)
	1664	δ_{as} (NH_2)
		ν_{as} (OCO)
	2930	ν_s (CH_2)
	2995	ν_{as} (CH_2)
3120		ν (NH_2)
3400	3488	ν (H_2O)

τ : torsion; δ : in-plane bending; γ : out-of-plane bending; ω : wagging; ν : stretching; r : rocking; t : twisting.

Structural characterization. The indexation of the two powder patterns viewed in **Figure 6** was performed through Le Bail refinements with the use of the Fullprof_Suite program. For the two compounds investigated, all the PXRD lines were taken into account, confirming that the samples were single phase. Similar results were obtained in each case and suggested a cubic system in the Pn-3 space group, with a = 19.0302(1) Å, V = 6891.8(1) Å and a = 19.0365(1) Å and V = 6898.6(1) $Å^3$.

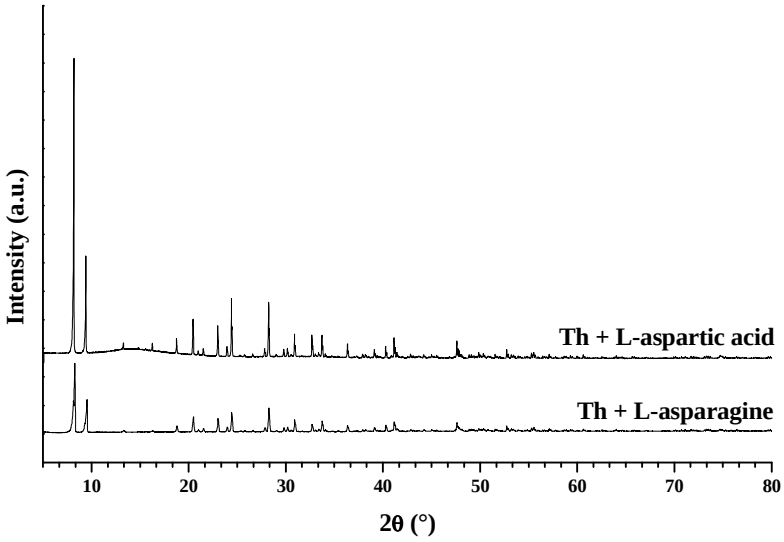

Figure 6. PXRD patterns of the precipitates obtained after complexation of thorium solution with L-asparagine and L-aspartic acid (Cu $K\alpha_{1,2}$ radiation, λ = 1.54184 Å).

Attempts to solve the crystal structure were unsuccessful because of the presence of a heavy element (thorium) which preclude the collection of capillary PXRD patterns. However, four thorium atoms were localized within the unit cell. By considering the general formula proposed above of $Th(C_4NO_4H_6)_4.nH_2O$, the calculated crystal density was evaluated to 0.8 $g.cm^{-3}$ which may suggest the existence of a porous crystal structure. Moreover, regarding the tetravalent oxidation state of thorium and the structural hypotheses suggested from ^{13}C NMR results and spectroscopic analyses, only one carboxylate function of the complexing agent should be linked to the thorium atom, with the rest of its coordination sphere completed by water molecules. Thus, the whole crystal structure could consist of isolated (0D) Th-polyhedra separated by aspartate molecules. However, single crystals or powder synchrotron data (capillary) are still needed in order to determine the complete crystal structure, which is the main objective of forthcoming studies.

3.2. Thermal vs hydrothermal decomposition

The thermal decomposition of thorium aspartate was first studied by the means of TG/DT analyses (**Figure 7**). The variation of the relative weight loss versus temperature exhibited several steps leading to the final formation of ThO_2 after heating above 500°C. A first weight loss of about 9% was observed between room temperature and 200°C. It was assigned to the dehydration of the initial sample. Also, it must be noticed that a small exothermic peak was detected around 200°C on the DT signal, without any associated weight loss. On this basis, it could correspond to a phase transition of the anhydrous thorium aspartate towards a high temperature form. The decomposition of the aspartate fragments further started from 260°C. The focus presented in **Figure 7** clearly shows that the conversion into ThO_2 occurs through two distinct and successive steps, although very close in temperature (DT peaks maximum at 270 and 275°C). For this reason, it appeared very difficult to assign precisely the corresponding weight losses which are probably overlapping. However, one can suggest that the first step (associated to an additional weight loss of about 10%) could be assigned to the departure of nitrogen-based species while the second (41% weight loss) could correspond to the elimination of the organic part as CO and CO_2. As this last step occurred very quickly, with the loss of more than the half of the powder mass within 10°C, it surely did not allow to fully eliminate the carbon content within the sample. Indeed, a residual weight loss of about 5% was recorded between 280 and 600°C, which corresponds to the elimination of amorphous carbon still present within the oxide sample. Such phenomenon was already stated in several actinide carboxylates, including oxalates [40-42]. The final temperature of oxide formation and the amount of residual carbon within the sample is thus strongly dependent on the atmosphere used during the thermal conversion, the best results being obtained in oxidizing conditions (typically in air) [29]. These results then underline once again the necessity to control the conversion of organic precursors toward final oxide sample, particularly in the perspective of sintering where the presence of carbon residues might modify the densification behavior.

Finally, the total weight loss recorded during the conversion of thorium aspartate between room temperature and 600°C, *i.e.* 67%, accounts for 4 water molecules and 4 aspartate units per thorium atom, leading to a general formula of $Th(C_4NO_4H_6)_4.4H_2O$, *i.e.* thorium aspartate tetrahydrate. Such a formulation was supported by the chemical analyses performed on the powdered precursors, which led to experimental elementary composition (wt.%(O) = 35.2 ± 3.5 % and wt.%(N) = 5.0 ± 0.5 %) very close to that calculated (wt.%(O) =

38% and wt.%(N) = 6%). It is also in very good agreement with the hypothesis of the presence of monodentate aspartate ligand as suggested from the results obtained by ^{13}C NMR.

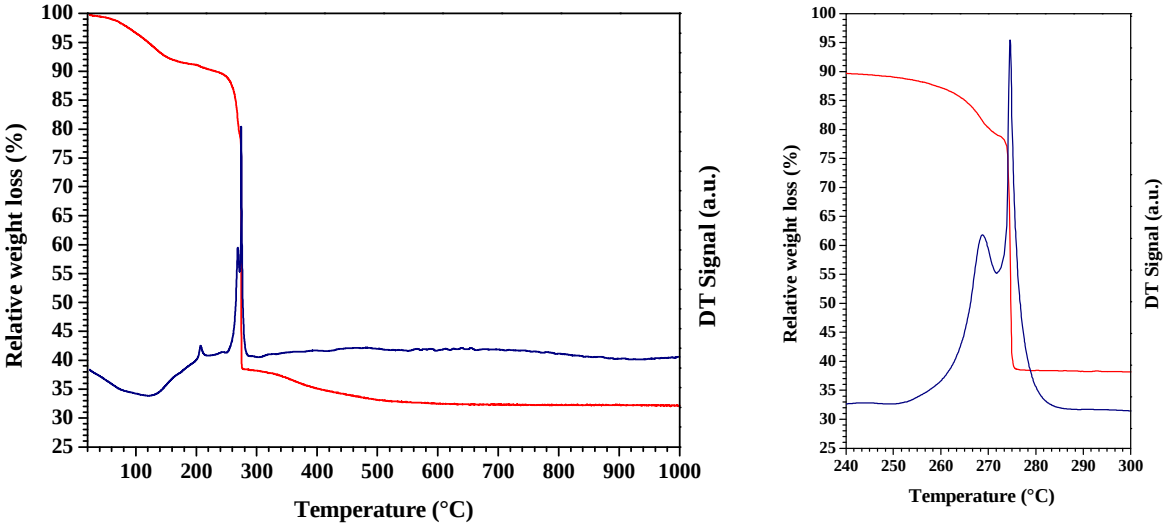

Figure 7. Thermogravimetric (red) and differential thermal analyses (blue) of thorium aspartate with focus on the 240-300°C range.

In parallel, the conversion of thorium aspartate tetrahydrate was monitored from a morphological point of view using *in situ* High Temperature Environmental Scanning Electron Microscopy (HT-ESEM) observations. These latter were performed during the heat treatment in air of a small amount of $Th(C_4NO_4H_6)_4.4H_2O$ up to 800°C under a pressure of 300 Pa (**Figure 8**, associated video supplied as supplementary material). The oxide obtained after heating at 800°C presents exactly the same morphology than the initial sample. The conversion of the thorium aspartate tetrahydrate then appeared to be pseudomorphic. Such feature was already stated for several others precursors of actinide dioxides, and particularly for oxalate compounds [43]. This shape stability then could be considered as a general characteristic of An-based coordination polymers and molecular complexes, and is of particular interest if one wants to control precisely the morphology of the oxide powder from its preparation method.

The good resolution offered by HT-ESEM, associated to image stability, also allowed us to extract quantitative data such as grains size. Based on the hypothesis of ideal bipyramids, the volume of a grain was then plotted versus temperature and compared with the relative weight loss obtained from TG analysis (**Figure 8**). If the final relative shrinkage appeared to be very close to weight loss (*i.e.* decrease of approximately 70% in volume), the

trend in the variation of V/V_0 versus temperature significantly differs from the TG curve. Two main steps were considered in the volume variation. First, shrinkage of about 25% was observed between room temperature and 230°C, which could be correlated to the dehydration of the initial compound (**Figure 7**, ① to ②).

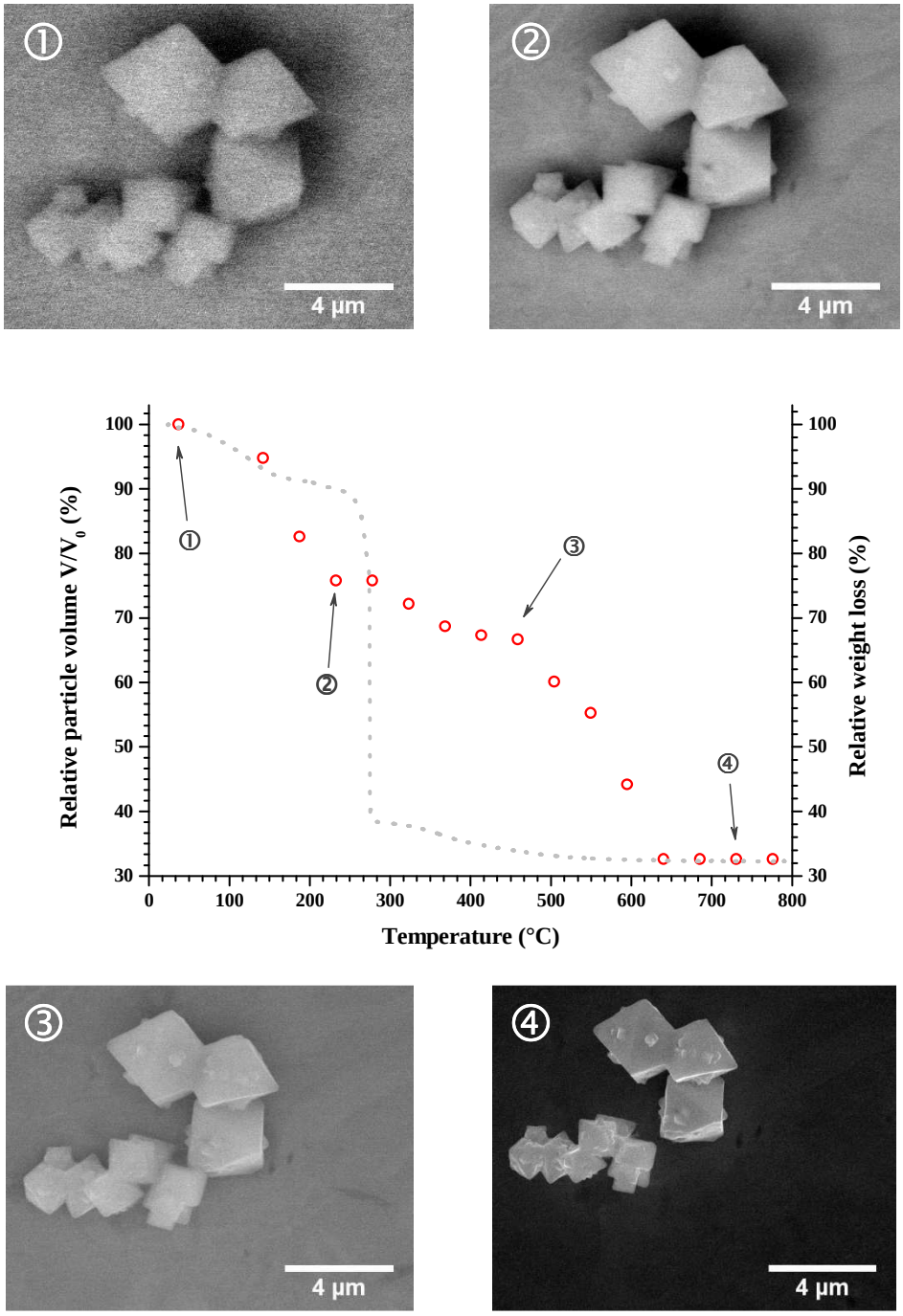

Figure 8. HT-ESEM observations performed during the thermal conversion of thorium aspartate tetrahydrate and associated evolution of a particle size compared to the weight loss measured by TGA.

More surprisingly, the decomposition of the organic species, associated to an important weight loss of about 60%, was not found to lead to a drastic decrease of the sample volume since only a 10% shrinkage was measured up to 450°C (**Figure 7**, ② to ③). Based on this observation, and on the results reported in the literature for the decomposition of thorium oxalate [28], one can assume that the decomposition of the organic architecture into CO and CO_2 led to the formation of mesopores (typically of a few nanometers) within the initial bipyramids. Conversely, a strong volume drop occurred at higher temperature (450-650°C), and was correlated to the elimination of this porosity, accompanied by the growth of the crystallites constituting the grains [44] (**Figure 7**, ③ to ④).

Simultaneously, several experiments were undertaken in order to operate the conversion of thorium aspartate tetrahydrate into ThO_2 through hydrothermal treatment. Indeed, several authors already reported the formation of metal oxides after hydrothermal decomposition of carboxylate complexes, including nitrogenous [45, 46] or oxalate [47, 48] compounds. The experimental protocol designed for the precipitation of $Th(C_4NO_4H_6)_4.4H_2O$ was then repeated, starting either from mixtures of thorium and L-asparagine or L-aspartic acid, now considering a temperature of 200°C. The ESEM micrographs of the samples obtained (**Figure 9**) revealed a complete modification of the morphology compared to the operating conditions initially defined for the synthesis of thorium aspartate tetrahydrate (hydrothermal treatment of 24 hours at 160°C). Moreover, some differences were detected depending on the nature of the complexing reagent used.

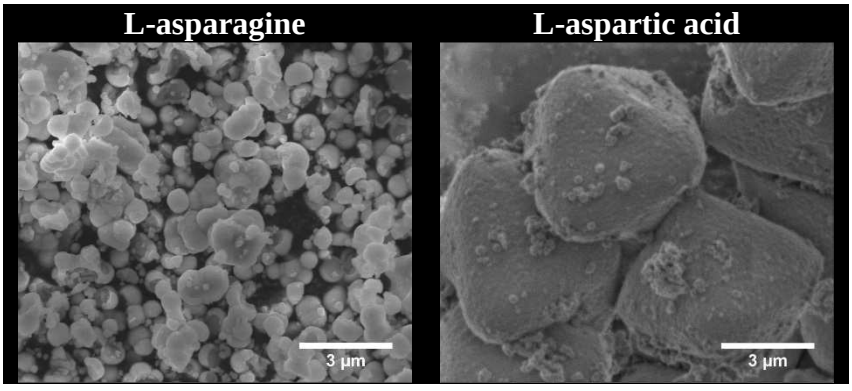

Figure 9. ESEM micrographs of the samples prepared after 24h of hydrothermal treatment at 200°C.

When using L-asparagine, spherical aggregates of small particles were formed, with a size ranging from a few hundredths nanometers to 1-2 µm. One can suggests that the

formation of such microspheres could be related to the hydroxylation of actinides, which is well-known to be the first step leading to the formation of colloids in solution, which further aggregate to yield nanoparticles [49, 50]. In our work, the hydroxylation of thorium probably proceeded through the increase of pH in the reacting mixture consequently to the release of ammonia during the decomposition of asparagine into aspartic acid. Also, remaining aspartic acid in solution might act as a shape modulator which orientates the growth/aggregation in a preferential way. A comparable process was indeed recently observed during the formation of $UO_2.nH_2O$ microspheres [20].

When using L-aspartic acid, the morphology of the sample obtained appeared closer to the initial bipyramids initially prepared at 160°C, as relics of edges and vertices were still viewed on the micrograph. However, the surface appeared to be composed of multiple rounded submicrometric crystallites, then confirming the decomposition of the aspartate compound. In this case, the formation of ThO_2 then most probably proceeded through a thermal decomposition of the ligand, which can be put in parallel with that evidenced during TG analyses.

In a last step, the samples formed both from hydrothermal and thermal decomposition of $Th(C_4NO_4H_6)_4.4H_2O$ thorium aspartate tetrahydrate were characterized by PXRD. All the patterns gathered in **Figure 10** confirmed the formation of thorium oxides exhibiting the characteristic PXRD lines of the well-known fluorite-type structure of ThO_2 (cubic, Fm-3m space group) [51]. However, different crystallization states were evidenced depending on the samples. Obviously, the samples prepared through decomposition under hydrothermal conditions were associated to wider PXRD peaks, which could be linked to the nanosized nature of the powder, in good agreement with the observation of small particles composing larger aggregates on SEM micrographs. This feature was also confirmed by the Rietveld refinement of the patterns, which led to average crystallite size values close to 40 nm whatever the complexing reactant used during the hydrothermal process (**Table 2**). Also, it is interesting to note that the values determined for the unit cell parameter and volume were slightly above those usually reported for ThO_2 (for example a = 5.598 Å from Hubert *et al.* [51]). Such discrepancy probably underlines the presence of water and/or residual carbon within the oxide structure, that appears in good agreement with the observations made by several authors during the direct preparation of actinide dioxides in solution [49, 52]. The general formula of the oxides obtained by this way could thus be written as $ThO_2.nH_2O$.

On the other hand, the oxides obtained after thermal conversion of the initial thorium aspartate tetrahydrate exhibited unit cell parameters in very good agreement with the referenced data. As already suggested from TGA data, firing of the powders at high temperature then ensured the full dehydration then decomposition of the aspartate entities. However, for the lowest temperature considered (i.e. 600°C), the conversion was not associated with a significant increase of the average crystallite size, which remains in the same order of magnitude than that measured for samples prepared through hydrothermal conversion. Conversely, the PXRD pattern collected after heat treatment at 1000°C revealed intense and narrow XRD lines which were associated to the strong increase of the crystallite size by a factor of 8-10 (i.e. typically from 40 nm to about 650 nm).

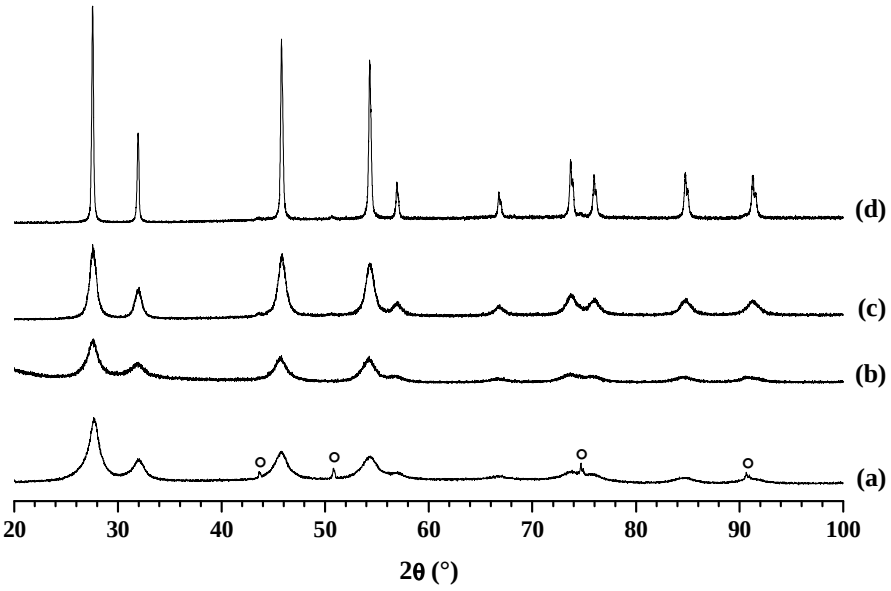

Figure 10. PXRD patterns collected from the oxide samples obtained through hydrothermal conversion (T = 200°C, t = 24 hours) of thorium aspartate formed from L-asparagine (a) and L-aspartic acid (b) and through thermal conversion (6h – air atmosphere) at 600°C (c) and 1000°C (d). PXRD peaks from the sample holder are indicated by a circle (PDF file #00-023-0298).

The residual amount of carbon within ThO_2 samples was also evaluated since it could impact the physico-chemical properties of the oxide powder, and particularly its ability to sintering [29, 53]. In this framework, very different results were obtained depending on the conversion method considered. First, the hydrothermal conversion from a mixture of thorium and L-asparagine was found to yield to the highest carbon content, which exceeded 1 wt.%.

Such a high value probably arose from the sorption of asparagine/aspartic acid molecules onto the thorium oxides / oxo-hydroxides colloids initially formed by hydrolysis, which further remain trapped within the aggregates. As the use of L-aspartic acid favored the thermal decomposition of the initial aspartate complex, the residual carbon content in the resulting hydrated oxide then appeared much lower (around 0.3 wt.%). Moreover, this value was found to be in good agreement with that obtained after thermal conversion at 600°C. The decomposition of the thorium aspartate then yielded to similar thorium oxides in terms of crystallization state and residual carbon content, either when performing hydrothermal conditions in solution or using solid state route. However, if one really wants to obtain an oxide compound exhibiting a very-low carbon content (typically under 100 ppm), a heating step at high temperature seems to be required.

Table 2. Unit cell parameters, average crystallite size and residual carbon content of thorium oxide samples produced by hydrothermal or thermal conversion of thorium aspartate.

Sample	**a (Å)**	**V (Å^3)**	**Crystallite size (nm)**	**Carbon wt.%**
Hydrothermal conversion – 200°C				
From L-asparagine	5.6192(2)	177.43(1)	42 ± 1	1.250
From L-aspartic acid	5.6178(3)	177.29(2)	44 ± 3	0.270
Thermal conversion – 6 h				
600°C	5.6026(2)	175.86(1)	82 ± 5	0.090
1000°C	5.5964(1)	175.28(1)	640 ± 40	0.005

4. Conclusions

The synthesis of an original thorium-based molecular compound was performed using two different wet-chemistry routes, involving either L-asparagine or L-aspartic acid as a complexing reagent. Both yielded to thorium aspartate tetrahydrate, *i.e.* $Th(C_4NO_4H_6)_4.4H_2O$, which precipitated as micrometric bipyramidal single crystals. Complete characterization of this compound allowed to confirm its formulation, and particularly the monodentate character of the aspartate group. Also, PXRD data led to specify a potential cubic lattice (Pn-3 space group) for this compound, although full structural resolution was precluded by the presence of heavy thorium atoms.

The conversion of thorium aspartate tetrahydrate into thorium dioxide was obtained through classical high temperature heat treatment or by the means of hydrothermal reaction. These various methods resulted in wide range of oxide characteristics, both in terms of morphology, chemical composition and crystallization state. On the one hand, thermal treatment provided a pseudomorphic conversion which kept the initial bipyramidal morphology. Such a method also favored the increase of the average crystallite size, as well as the complete elimination of the residual carbon content. On the other hand, hydrothermal conversion could be used to tune the morphology of the final oxide, since $ThO_2.nH_2O$ microspheres were prepared when starting from L-asparagine. Even if this process was associated to higher carbon contents, the hydrothermal conversion of metallic carboxylates then appeared as an interesting option to control the final physico-chemical properties of the resulting oxide powders. Also, two-step protocols involving both hydrothermal and thermal treatments could be tested in order to get improved control over both microstructural and chemical features of the final oxide. One can then expect to enhance significantly the sintering capability of the oxide powders produced, either when dealing with ThO_2 or derived solid solutions.

Acknowledgements

Authors would like to thank J. Ravaux and J. Lautru (ICSM/L2ME) and C. Rey (ICSM/LNER) for their help during SEM observations and LECO analyses. They are also grateful to the Materials Federative Project included in the NEEDS program (Nucléaire, Energie, Environnement, Déchets, Société) of CNRS for its continuous financial support.

References

[1] T. Loiseau, I. Mihalcea, N. Henry, C. Volkringer, The crystal chemistry of uranium carboxylates, Coordin Chem Rev 266 (2014) 69-109.

[2] A. Handschuh, S. Dubois, S. Vaudez, S. Grandjean, G. Leturcq, F. Abraham, Direct carbothermic reduction of actinide oxalates: Example of Nd(III) oxalate-carbon mixtures conversion, J Nucl Mater 385(1) (2009) 186-188.

[3] F. Abraham, B. Arab-Chapelet, M. Rivenet, C. Tamain, S. Grandjean, Actinide oxalates, solid state structures and applications, Coord. Chem. Rev. 266-267 (2014) 28-68.

[4] B. Arab-Chapelet, S. Grandjean, G. Nowogrocki, F. Abraham, Synthesis and characterization of mixed An(IV)An(III) oxalates (An(IV) = Th, Np, U or Pu and An(III) = Pu or Am), J Nucl Mater 373(1-3) (2008) 259-268.

[5] R.M. Orr, H.E. Sims, R.J. Taylor, A review of plutonium oxalate decomposition reactions and effects of decomposition temperature on the surface area of the plutonium dioxide product, J Nucl Mater 465 (2015) 756-773.

[6] V. Tyrpekl, J.F. Vigier, D. Manara, T. Wiss, O.D. Blanco, J. Somers, Low temperature decomposition of U(IV) and Th(IV) oxalates to nanograined oxide powders, J Nucl Mater 460 (2015) 200-208.

[7] G.D. White, L.A. Bray, P.E. Hart, Optimization of Thorium Oxalate Precipitation Conditions Relative to Derived Oxide Sinterability, J Nucl Mater 96(3) (1981) 305-313.

[8] K. Ananthasivan, S. Anthonysamy, A. Singh, P.R.V. Rao, De-agglomeration of thorium oxalate - a method for the synthesis of sinteractive thoria, J Nucl Mater 306(1) (2002) 1-9.

[9] D. Horlait, F. Lebreton, A. Gauthe, M. Caisso, B. Arab-Chapelet, S. Picart, T. Delahaye, Americium-based oxides: Dense pellet fabrication from co-converted oxalates, J Nucl Mater 444(1-3) (2014) 181-185.

[10] C. Falaise, A. Assen, I. Mihalcea, C. Volkringer, A. Mesbah, N. Dacheux, T. Loiseau, Coordination polymers of uranium(IV) terephthalates, Dalton T 44(6) (2015) 2639-2649.

[11] C. Falaise, J.S. Charles, C. Volkringer, T. Loiseau, Thorium Terephthalates Coordination Polymers Synthesized in Solvothermal DMF/H_2O System, Inorg Chem 54(5) (2015) 2235-2242.

[12] C. Volkringer, I. Mihalcea, J.F. Vigier, A. Beaurain, M. Visseaux, T. Loiseau, Metal-Organic-Framework-Type 1D-Channel Open Network of a Tetravalent Uranium Trimesate, Inorg Chem 50(23) (2011) 11865-11867.

[13] T. Demars, M. Boltoeva, N. Vigier, J. Maynadie, J. Ravaux, C. Genre, D. Meyer, From Coordination Polymers to Doped Rare-Earth Oxides, Eur J Inorg Chem 2012(24) (2012) 3875-3884.

[14] M. Pradhan, S. Sarkar, A.K. Sinha, M. Basu, T. Pal, Morphology controlled uranium oxide hydroxide hydrate for catalysis, luminescence and SERS studies, Crystengcomm 13(8) (2011) 2878-2889.

[15] Q. Wang, G.D. Li, S. Xu, J.X. Li, J.S. Chen, Synthesis of uranium oxide nanoparticles and their catalytic performance for benzyl alcohol conversion to benzaldehyde, J Mater Chem 18(10) (2008) 1146-1152.

[16] J.E. Kelly, Generation IV International Forum: A decade of progress through international cooperation, Progress in Nuclear Energy 77 (2014) 240-246.

[17] K. Anantharaman, V. Shivakumar, D. Saha, Utilisation of thorium in reactors, J Nucl Mater 383(1-2) (2008) 119-121.

[18] R.K. Sinha, A. Kakodkar, Design and development of the AHWR - the Indian thorium fuelled innovative nuclear reactor, Nucl Eng Des 236(7-8) (2006) 683-700.

[19] D. Hudry, C. Apostolidis, O. Walter, T. Gouder, E. Courtois, C. Kubel, D. Meyer, Non-aqueous Synthesis of Isotropic and Anisotropic Actinide Oxide Nanocrystals, Chem-Eur J 18(27) (2012) 8283-8287.

[20] G.I. Nkou Bouala, N. Clavier, R. Podor, J. Cambedouzou, A. Mesbah, H.P. Brau, J. Léchelle, N. Dacheux, Preparation and characterisation of uranium oxides with spherical shapes and hierarchical structures, Crystengcomm 16 (2014) 6944-6954.

[21] L. Wang, R. Zhao, C.Z. Wang, L.Y. Yuan, Z.J. Gu, C.L. Xiao, S.A. Wang, X.W. Wang, Y.L. Zhao, Z.F. Chai, W.Q. Shi, Template-Free Synthesis and Mechanistic Study of Porous Three-Dimensional Hierarchical Uranium-Containing and Uranium Oxide Microspheres, Chem-Eur J 20(39) (2014) 12655-12662.

[22] D. Hudry, J.C. Griveau, C. Apostolidis, O. Walter, E. Colineau, G. Rasmussen, D. Wang, V.S.K. Chakravadhaluna, E. Courtois, C. Kubel, D. Meyer, Thorium/uranium mixed oxide nanocrystals: Synthesis, structural characterization and magnetic properties, Nano Res 7(1) (2014) 119-131.

[23] L. Wang, R. Zhao, X.W. Wang, L. Mei, L.Y. Yuan, S.A. Wang, Z.F. Chai, W.Q. Shi, Size-tunable synthesis of monodisperse thorium dioxide nanoparticles and their performance on the adsorption of dye molecules, Crystengcomm 16(45) (2014) 10469-10475.

[24] Y. Andres, H.J. MacCordick, J.C. Hubert, Selective biosorption of thorium ions by an immobilized mycobacterial biomass, Appl Microbiol Biot 44(1-2) (1995) 271-276.

[25] D. Humelnicu, G. Drochioiu, K. Popa, Bioaccumulation of thorium and uranyl ions on Saccharomyces cerevisiae, J Radioanal Nucl Ch 260(2) (2004) 291-293.

[26] Z.R. Shen, J.G. Wang, P.C. Sun, D.T. Ding, T.H. Chen, Fabrication of lanthanide oxide microspheres and hollow spheres by thermolysis of pre-molding lanthanide coordination compounds, Chem Commun (13) (2009) 1742-1744.

[27] M. Yang, Z.R. Shen, T.H. Chen, H.C. Bi, B. Yang, W. Xu, Induced morphology control of Ln-asparagine coordination polymers from the macro to nanoscopic regime in polar solvent-water mixtures, Dalton T 42(4) (2013) 1174-1179.

[28] L. Claparede, N. Clavier, N. Dacheux, A. Mesbah, J. Martinez, S. Szenknect, P. Moisy, Multiparametric Dissolution of Thorium-Cerium Dioxide Solid Solutions, Inorg Chem 50(22) (2011) 11702-11714.

[29] J. Martinez, N. Clavier, T. Ducasse, A. Mesbah, F. Audubert, B. Corso, N. Vigier, N. Dacheux, From uranium(IV) oxalate to sintered UO_2: Consequences of the powders' thermal history on the microstructure, J Eur Ceram Soc 35(16) (2015) 4535-4546.

[30] D. Horlait, F. Tocino, N. Clavier, N. Dacheux, S. Szenknect, Multiparametric study of $Th_{1-x}Ln_xO_{2-x/2}$ mixed oxides dissolution in nitric acid media, J Nucl Mater 429(1-3) (2012) 237-244.

[31] M. Simonnet, N. Barre, R. Drot, C. Le Naour, V. Sladkov, S. Delpech, Multiparametric study of thorium oxide dissolution in aqueous media, Radiochim Acta 104(10) (2016) 691-700.

[32] R.F. Lumb, A.E. Martell, Metal Chelating Tendencies of Glutamic and Aspartic Acids, J Phys Chem-Us 57(7) (1953) 690-693.

[33] J. Schindelin, I. Arganda-Carreras, E. Frise, V. Kaynig, M. Longair, T. Pietzsch, S. Preibisch, C. Rueden, S. Saalfeld, B. Schmid, J.Y. Tinevez, D.J. White, V. Hartenstein, K. Eliceiri, P. Tomancak, A. Cardona, Fiji: an open-source platform for biological-image analysis, Nat Methods 9(7) (2012) 676-682.

[34] P. Thompson, D.E. Cox, J.B. Hastings, Rietveld refinement of Debye-Scherrer synchrotron X-ray data from Al_2O_3, Journal of Applied Crystallography 20 (1987) 79-83.

[35] C. Frontera, J. Rodriguez-Carvajal, FullProf as a new tool for flipping ratio analysis, Physica B: Condensed Matter 335(1-4) (2003) 219-222.

[36] L.Y. Chen, Z.D. Zhang, Biomolecule-Assisted Synthesis of $In(OH)_3$ Hollow Spherical Nanostructures Constructed with Well-Aligned Nanocubes and Their Conversion into C-In_2O_3, J Phys Chem C 112(48) (2008) 18798-18803.

[37] J. Casado, J.T.L. Navarrete, F.J. Ramirez, Infrared and Raman-Spectra of L-Asparagine and L-Asparagine-D(5) in the Solid-State, J Raman Spectrosc 26(11) (1995) 1003-1008.

[38] J.T.L. Navarrete, V. Hernandez, F.J. Ramirez, IR and Raman-Spectra of L-Aspartic Acid and Isotopic Derivatives, Biopolymers 34(8) (1994) 1065-1077.

[39] O.V. Cabral, C.A. Tellez, T. Giannerini, J. Felcman, Fourier-transform infrared spectrum of aspartate hydroxo-aqua nickel(II) complex and DFT-B3LYP/3-21G and 6-311G structural and vibrational calculations, Spectrochim Acta A 61(1-2) (2005) 337-345.

[40] S. Dash, R. Krishnan, M. Kamruddin, A.K. Tyagi, B. Raj, Temperature programmed decomposition of thorium oxalate hexahydrate, J Nucl Mater 295(2-3) (2001) 281-289.

[41] E. Oktay, A. Yayli, Physical properties of thorium oxalate powders and their influence on the thermal decomposition, J Nucl Mater 288(1) (2001) 76-82.

[42] M.T. Aybers, Kinetic study of the thermal decomposition of thorium oxalate dihydrate, J Nucl Mater 252(1-2) (1998) 28-33.

[43] D. Horlait, N. Clavier, N. Dacheux, R. Cavalier, R. Podor, Synthesis and characterization of $Th_{1-x}Ln_xO_{2-x/2}$ mixed-oxides, Mater Res Bull 47(12) (2012) 4017-4025.

[44] G.I. Nkou Bouala, N. Clavier, J. Lechelle, A. Mesbah, N. Dacheux, R. Podor, *In situ* HT-ESEM study of crystallites growth within CeO_2 microspheres, Ceramics International 41(10) (2015) 14703-14711.

[45] M.A. Verges, M. Martinez, E. Matijevic, Synthesis and Characterization of Zinc Ferrite Particles Prepared by Hydrothermal Decomposition of Zinc Chelate Solutions, J Mater Res 8(11) (1993) 2916-2920.

[46] H. Nishizawa, T. Tani, K. Matsuoka, Crystal-Growth of Zno by Hydrothermal Decomposition of Zn-EDTA, J Am Ceram Soc 67(6) (1984) C98-C100.

[47] X.Z. Zhang, L.H. Yue, M. Wan, Y.F. Zheng, Synthesis of porous manganese oxides bars via a hydrothermal-decomposition method, Mater Chem Phys 124(1) (2010) 831-834.

[48] O. Walter, K. Popa, O. Dieste Blanco, Hydrothermal decomposition of actinide(IV) oxalates: a new aqueous route towards reactive actinide oxide nanocrystals, Open. Chem. 14(1) (2016) 170-174.

[49] V. Neck, J.I. Kim, Solubility and hydrolysis of tetravalent actinides, Radiochim Acta 89(1) (2001) 1-16.

[50] D. Rai, A.R. Felmy, J.L. Ryan, Uranium(IV) Hydrolysis Constants and Solubility Product of $UO_2.xH_2O$(am), Inorg Chem 29(2) (1990) 260-264.

[51] S. Hubert, J. Purans, G. Heisbourg, P. Moisy, N. Dacheux, Local structure of actinide dioxide solid solutions $Th_{1-x}U_xO_2$ and $Th_{1-x}Pu_xO_2$, Inorg Chem 45(10) (2006) 3887-3894.

[52] J. Martinez, N. Clavier, A. Mesbah, F. Audubert, X.F. Le Goff, N. Vigier, N. Dacheux, An original precipitation route toward the preparation and the sintering of highly reactive uranium cerium dioxide powders, J Nucl Mater 462 (2015) 173-181.

[53] K. Asakura, K. Takeuchi, Effect of residual carbon on the sintering behavior of MOX pellets, J Nucl Mater 348(1-2) (2006) 165-173.

Supplementary material

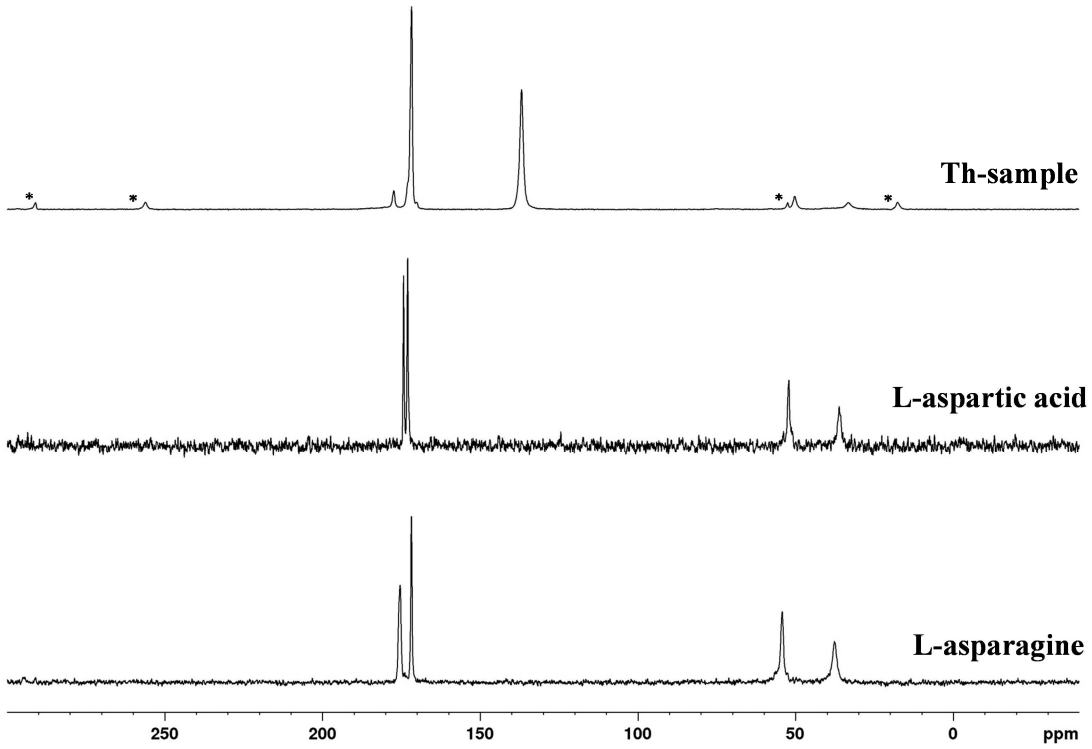

Figure S1. Solid state ^{13}C NMR CP-MAS spectra of L-asparagine, L-aspartic acid and Th-sample in the whole analysed range. Stars indicate spinning sidebands.

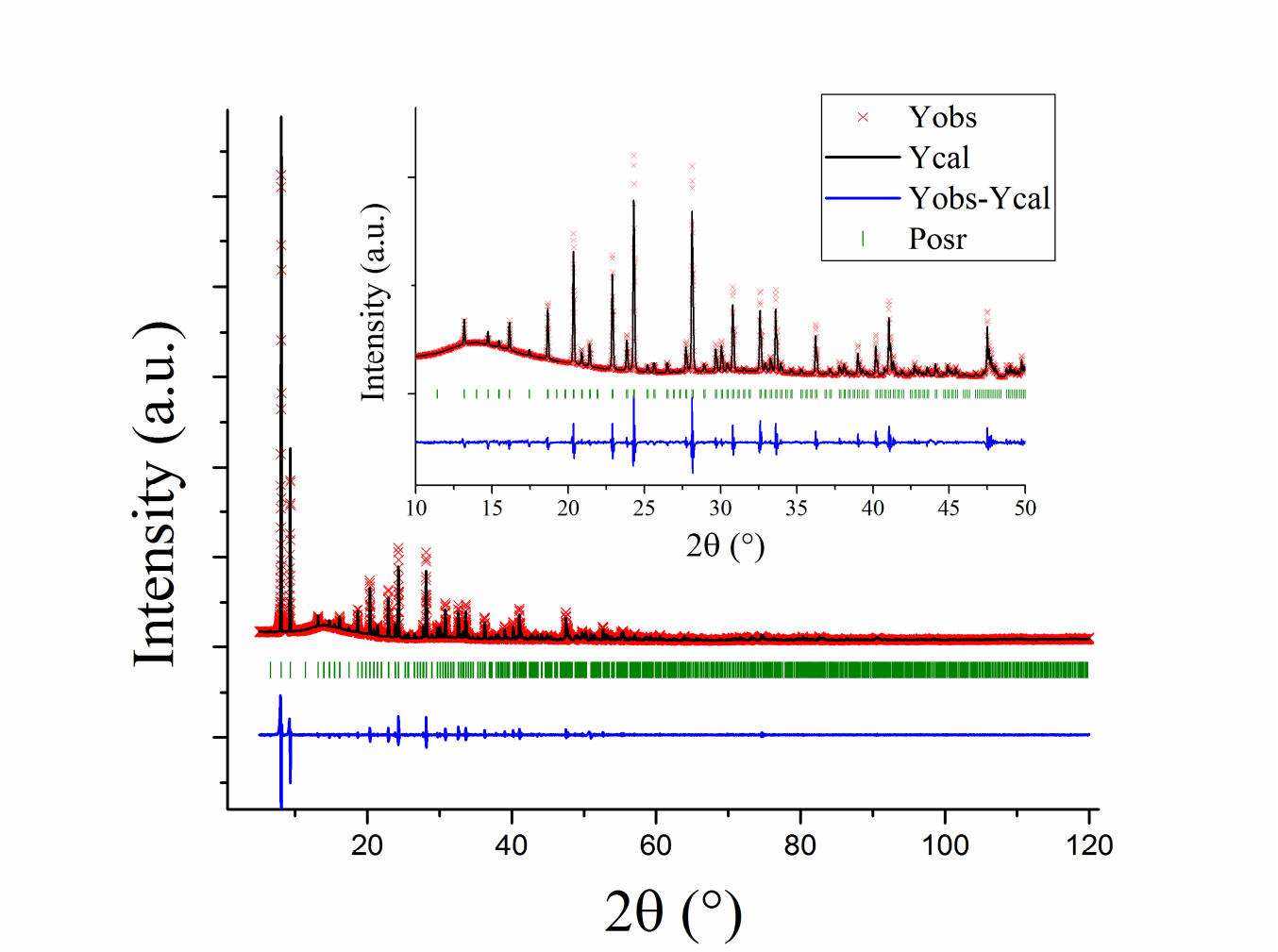

Figure S2. Le Bail refinement plot showing the observed, calculated and the difference for the thorium complex formed with L-aspartic acid.

Table S1. Band assignment of the ATR-FTIR and Raman spectra recorded from L-aspartic acid, based on the results of Navarrete *et al.* [16b].

ATR-FTIR (cm^{-1})	Raman (cm^{-1})	Assignment
408		τ (skel.)
446		δ (skel.)
	470	τ (NH_3^+)
551 652	552 663	δ (COOH)
598 752	600 747	δ (CO_2^-)
777	779	γ (OCO)
871	871	τ (CH_2)
896 988	902 990	ν (CC)
936	937	γ (OH)
1082	1083	ν (CN)
1117 1148	1121 1145	r (NH_3^+)
1246	1250	t (CH_2)
	1263 1406	ν (CO) + δ (OH)
1332 1359	1336 1360	δ (CH)
1418	1425	ν_s (CO_2^-)
1504	1506	δ_s (NH_3^+)
1596	1616	ν_{as} (CO_2)
1640	1635	δ_{as} (NH_3^+)
1684	1697	ν (C=O)
2948	2955	ν_s (CH_2)
	2997	ν (CH)
	3014	ν_{as} (CH_2)

τ : torsion; δ : in-plane bending; γ : out-of-plane bending; ω : wagging; ν : stretching; r : rocking; t : twisting.

Table S2. Band assignment of the ATR-FTIR and Raman spectra recorded from L-asparagine, based on the results of Casado *et al.* [16a].

ATR-FTIR (cm^{-1})	Raman (cm^{-1})	Assignment
410 537	414 541	τ (NH_3^+)
452	452	τ (skel.)
581 659		δ (CO_2^-)
629 680	661	δ ($CONH_2$)
754	754	γ (NCO)
761	764	γ (CO_2^-)
846		γ (NH_3^+)
877	877	τ (CH_2)
897 941 985	897 941 987	ν (CC)
1072	1072	ν (CN)
1112 1151 1165	1114 1155 1161	r (NH_3^+)
1246	1251	t (CH_2)
1264	1264	ω (CH_2)
1333 1354	1331 1355	δ (CH)
1395	1417	ν' (CN), amide III
1423		ν_s (CO_2^-)
1580	1561	
1490	1501	δ_s (NH_3^+)
1606	1622	ν' (CN), amide II
1641		ν (C=O), amide I
1673	1674	δ_{as} (NH_3^+)
	2943	ν_s (CH_2)
	2978	ν (CH)
	2990	ν_{as} (CH_2)
	3063	ν_s (NH_2)
3350	3353	ν_{as} (NH_2)

τ : torsion; δ : in-plane bending; γ : out-of-plane bending; ω : wagging; ν : stretching; r : rocking; t : twisting.